Detectability of patches in fractal textures for assessing Hölder exponent-based breast cancer risk evaluation

B. Pascal[1], H. Biermé[2,†]

† Partially supported by Grant ANR-19-CE40-0005 "*MISTIC*"
1. Nantes Université, École Centrale Nantes, CNRS, LS2N, UMR 6004, F-44000 Nantes, France barbara.pascal@cnrs.fr
2. Université de Tours, CNRS, UMR 7013, Institut Denis Poisson, France hermine.bierme@univ-tours.fr

Aims and contributions

Early detection of breast cancer is key to survival. The local Hölder exponent distribution in a mammogram enables to quantify breast tissue disruption, and hence to assess breast cancer risk. This work proposes a systematic study of the detectability of disrupted tissues embedded inside fatty vs. dense microenvironments leveraging simulated piecewise homogeneous fractal textures modeling breast tissues.

Contributions:

- Novel *filtered* fractional Brownian field (*filtered fBf*) model for stationary isotropic fractal textures.
- Simulations on synthetic piecewise homogeneous *filtered fBf* and fractional Gaussian field (*fGf*) textures: segmentation of a patch.
- Quantification of the detectability of simulated disrupted tissues $H_{\mathrm{p}} = 0.5$ in simulated fatty $H_{\mathrm{b}} = 0.3$ vs. dense $H_{\mathrm{b}} = 0.65$ tissues.

Outcomes:

- High detection performance for large patches of disrupted tissues in **fatty** environments, with a drop in accuracy for small patches.
- For **dense** environments detection performance are good and decrease slowly with the patch size.

Mammogram provided by **CompUMaine** from (Gerasimova-Chechkina et al., 2021, *Front. Physiol.*)

Fractal texture models

Fractional Brownian field (*fBf*)

$$\mathsf{B}_H(\underline{x}) = \int_{\mathbb{R}^2} \frac{\mathrm{e}^{-\mathrm{i}\underline{x}\cdot\underline{\omega}} - 1}{\|\underline{\omega}\|^{H+1}} \,\mathrm{d}\widetilde{\mathsf{W}}(\underline{\omega})$$

(Mandelbrot & Van Ness, 1968, *SIAM Rev.*)

Stationary self-similar fields

Fractional Gaussian field (*fGf*)

$$\mathsf{G}_H(\underline{x}) = \mathsf{B}_H(\underline{x} + \underline{e}_1) + \mathsf{B}_H(\underline{x} + \underline{e}_2) - 2\mathsf{B}_H(\underline{x})$$

(Pascal et al., 2021, *Appl. Comput. Harm. Anal.*)

Filtered fractional Brownian field

$$\mathsf{C}_H(\underline{x}) = \langle \mathsf{B}_H, \mathsf{u}_{\underline{x}} \rangle, \ \mathsf{u} \text{ high-pass filter}$$

$\langle \cdot, \cdot \rangle$ scalar product in $L^2(\mathbb{R}^2)$

Filter u from (Biermé et al., 2024, *Preprint*)

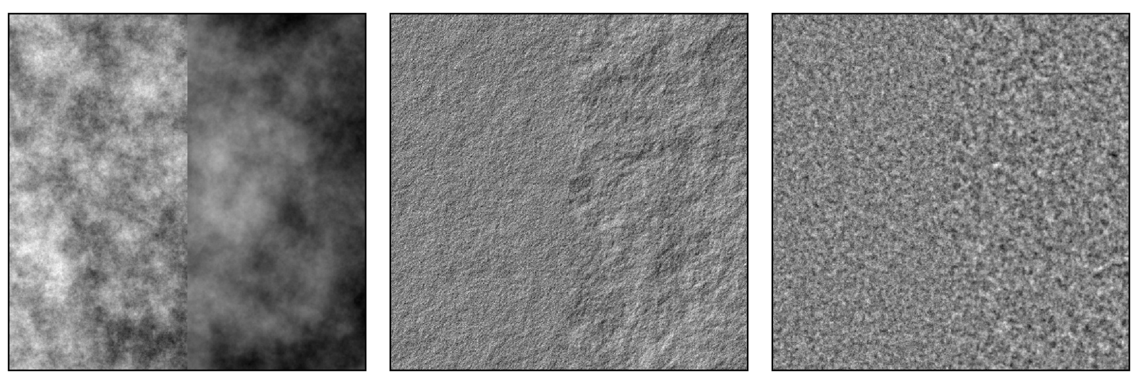

fBf B_H | *fGf* G_H | *Filtered fBf* C_H

Piecewise textures

Goal: Model breast local microenvironment.

Background: healthy microenvironment

- fatty tissues: $H_{\mathrm{b}} = 0.3$ (anticorrelated)
- dense tissues: $H_{\mathrm{b}} = 0.65$ (correlated)

Patch: disrupted tissues

- $H_{\mathrm{p}} = 0.5$ (uncorrelated)

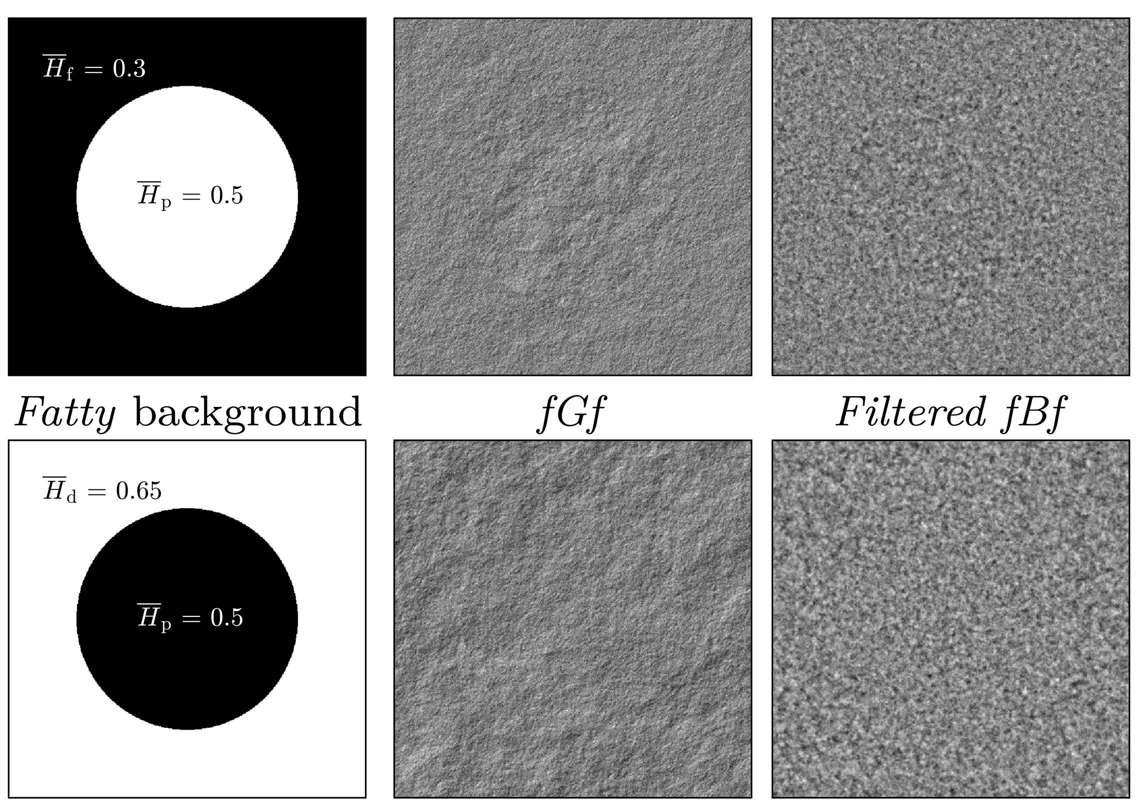

Fatty background | *fGf* | *Filtered fBf*

Dense background | *fGf* | *Filtered fBf*

Examples:

- images of 512×512 pixels;
- circular central patch: 30% of pixels;
- two configurations: two background types.

Hölder exponent-based texture segmentation

Local Hölder exponent: for a field $\mathsf{F} : \mathbb{R}^2 \to \mathbb{R}$ and $\underline{x}_0 \in \mathbb{R}^2$, $h(\underline{x}_0)$ defined as the largest exponent $\alpha > 0$ such that there exists a constant χ and a polynomial $\mathcal{P}_{\underline{x}_0}$ of degree lower than α such that for $\underline{x}$ in a neighborhood of $\underline{x}_0$: $|\mathsf{F}(x) - \mathcal{P}_{\underline{x}_0}(\underline{x})| \leq \chi \|\underline{x} - \underline{x}_0\|^{\alpha}$. For B_H, G_H and C_H: $\forall \underline{x} \in \mathbb{R}^2$, $h(\underline{x}) = H$.

Multiscale analysis and wavelet leaders: (Mallat, 1999, *Elsevier*) scaling function ϕ, mother wavelet $\psi \Longrightarrow \mathcal{Y}_{\mathsf{F}}^{(m)}(j, \underline{k}) = 2^{-j} \langle \mathsf{F}, \psi_{j,\underline{k}}^{(m)} \rangle$; *leaders*: $\mathcal{L}_{j,\underline{k}} = \sup\{|2^j \mathcal{Y}_{j',\underline{k}'}^{(m)}|,\ \lambda_{j',\underline{k}'} \subset 3\lambda_{j,\underline{k}}, m = 1, 2, 3\}$

$$\mathcal{L}_{j,\underline{k}} \simeq \eta(\underline{x}) 2^{jh(\underline{x})} \quad \text{as} \quad 2^j \to 0$$

(Jaffard, 2004, *Proc. Symp. Pure Math.*)

$\Longrightarrow$ *Linear Regression* on $\log_2 \mathcal{L}_{j,\underline{k}}$: local estimate $\widehat{h}^{\mathsf{LR}}(\underline{x})$.

Threshold Rudin-Osher-Fatemi estimator: 2D discrete gradient operator $\mathbf{D}$

$$\widehat{\boldsymbol{h}}^{\mathsf{ROF}} = \operatorname{argmin}_{\boldsymbol{h}} \|\boldsymbol{h} - \widehat{\boldsymbol{h}}^{\mathsf{LR}}\|_2^2 + \lambda \|\mathbf{D}\boldsymbol{h}\|_{2,1} \ \&\ \text{iterative thresholding} \Longrightarrow \mathcal{T}\widehat{\boldsymbol{h}}^{\mathsf{ROF}}.$$

(Nelson et al., 2016, *IEEE Trans. Image Process.*; B. Pascal et al., 2018, *ICASSP*);Cai et al., 2013, SIAM J. Imaging Sci.; Pascal et al., 2021, Appl. Comput. Harm. Anal.)

Stein-based automated parameter tuning: adapted Generalized Stein Unbiased Risk Estimate

$$\mathsf{GSURE}(\lambda) = \left\| \widehat{\boldsymbol{h}}^{\mathsf{ROF}} - \widehat{\boldsymbol{h}}^{\mathsf{LR}} \right\|^2 + 2\mathrm{Tr}\,(\boldsymbol{\mathcal{S}}\boldsymbol{J}) - \mathrm{Tr}(\boldsymbol{\mathcal{S}}) \ \text{not explicitly depending on } \overline{\boldsymbol{h}}$$

$\boldsymbol{J}$: Jacobian matrix of $\widehat{\boldsymbol{h}}^{\mathsf{ROF}}$ w.r.t. $\widehat{\boldsymbol{h}}^{\mathsf{LR}}$; $\boldsymbol{\mathcal{S}}$: empirical covariance of Gaussian noise corrupting $\widehat{\boldsymbol{h}}^{\mathsf{LR}}$.

Optimal $\lambda^\star$*:* minimization of $\mathsf{GSURE}(\lambda)$ with a BFGS scheme. (Pascal et al., 2020, Ann. Telecommun.)

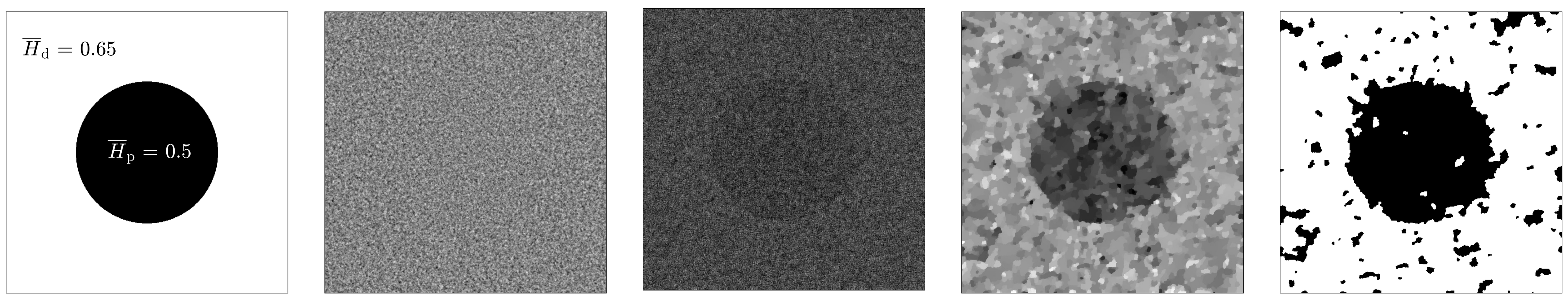

True $\overline{\boldsymbol{h}}$ | Piecewise texture | Lin. reg. $\widehat{\boldsymbol{h}}^{\mathsf{LR}}$ | ROF $\widehat{\boldsymbol{h}}^{\mathsf{ROF}}$ | T-ROF $\mathcal{T}\widehat{\boldsymbol{h}}^{\mathsf{ROF}}$

Numerical experiments: detectability of disrupted tissues

Detection performance criteria: F-score defined as $\mathsf{F}_1^{-1} = \mathsf{precision}^{-1} + \mathsf{recall}^{-1}$

- $\mathsf{precision}$: proportion of pixels segmented in the central patch indeed belonging to it;
- recall: proportion of pixels originally belonging to the central patch and correctly segmented.

$\Longrightarrow$ The larger $\mathsf{F}_1 \in [0, 1]$ the better the segmentation in terms of both errors of types I and II.

Two configurations: patch of disrupted tissues embedded in *fatty* vs. *dense* background; for each

- eight *relative* patch sizes $\{2\%, 5\%, 10\%, 15\%, 20\%, 30\%, 40\%, 50\%\}$,
- three image resolutions $N \in \{256, 512, 1024\}$,
- two synthetic texture models: *fGf* vs. *filtered fBf*,

$\Longrightarrow$ F_1 score average and 95% confidence regions computed on 10 texture realizations.

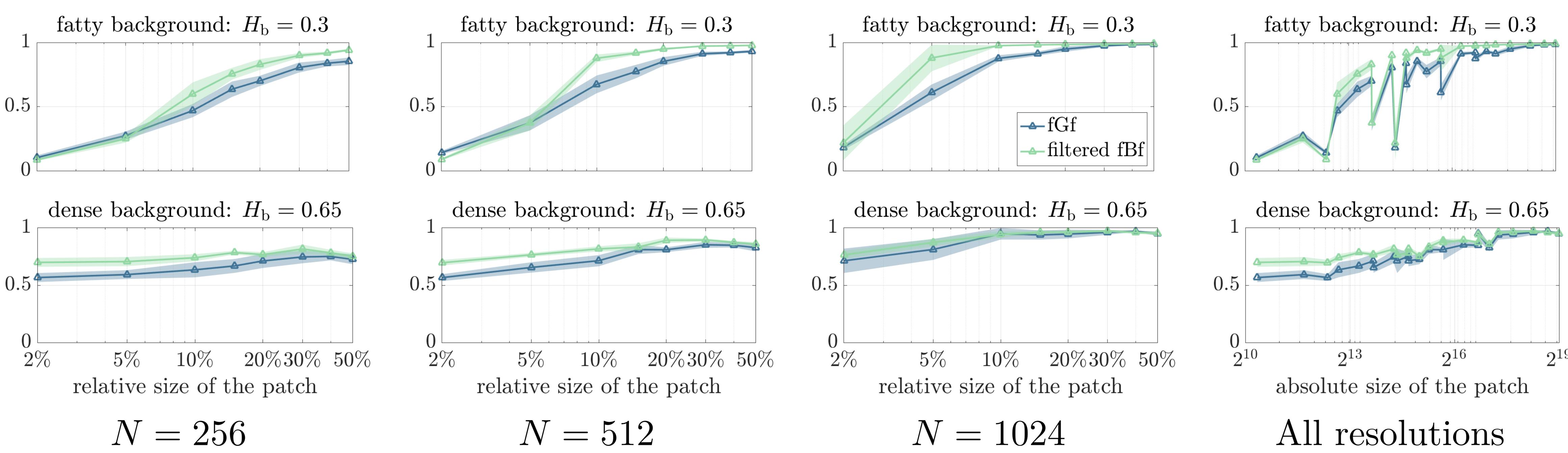

$N = 256$ | $N = 512$ | $N = 1024$ | All resolutions

Perspectives

- Detectability of disrupted tissues in *anistropic* textures (Richard & Biermé, 2010, *J. Math. Imaging Vis.*),
- Confidence level on Hölder exponent-based risk cancer assessment on real datasets, VinDr-Mammo.